The Meteoritical Society

Meteoritics & Planetary Science 45, Nr 8, 1243–1257 (2010)
doi: 10.1111/j.1945-5100.2010.01078.x

Effect of silicon on trace element partitioning in iron-bearing metallic melts

Nancy L. CHABOT[1*], Trevor M. SAFKO[2], and William F. McDONOUGH[3]

[1]Johns Hopkins University Applied Physics Laboratory, 11100 Johns Hopkins Road, Laurel, Maryland 20723, USA
[2]Villanova University, Villanova, Pennsylvania 19085, USA
[3]Department of Geology, University of Maryland, College Park, Maryland 20742, USA
[*]Corresponding author. E-mail: Nancy.Chabot@jhuapl.edu

(Received 23 December 2009; revision accepted 27 May 2010)

Abstract–Despite the fact that Si is considered a potentially important metalloid in planetary systems, little is known about the effect of Si in metallic melts on trace element partitioning behavior. Previous studies have established the effects of S, C, and P, nonmetals, through solid metal/liquid metal experiments in the corresponding Fe binary systems, but the Fe-Si system is not appropriate for similar experiments because of the high solubility of Si in solid metal. In this work, we present the results from 0.1 MPa experiments with two coexisting immiscible metallic liquids in the Fe-S-Si system. By leveraging the extensive available knowledge about the effect of S on trace element partitioning behavior, we explore the effect of Si. Results for 22 trace elements are presented. Strong Si avoidance behavior is demonstrated by As, Au, Ga, Ge, Sb, Sn, and Zn. Iridium, Os, Pt, Re, Ru, and W exhibit weak Si avoidance tendencies. Silicon appears to have no significant effect on the partitioning behaviors of Ag, Co, Cu, Cr, Ni, Pd, and V, all of which had similar partition coefficients over a wide range of Si liquid concentrations from Si-free to 13 wt%. The only elements in our experiments to show evidence of a potentially weak attraction to Si were Mo and Rh. Applications of the newly determined effects of Si to problems in planetary science indicate that (1) The elements Ni, Co, Mo, and W, which are commonly used in planetary differentiation models, are minimally affected by the presence of Si in the metal, especially in comparison to other effects such as from oxygen fugacity. 2) Reduced enstatite-rich meteorites may record a chemical signature due to Si in the metallic melts during partial melting, and if so, elements identified by this study as having strong Si avoidance may offer unique insight into unraveling the history of these meteorites.

INTRODUCTION

The composition of metallic melts can have important consequences on the chemical evolution of planetary bodies. As small, asteroid-sized bodies were heated and melted in the early solar system, the composition of the resulting metallic melts influenced the distribution of elements in these bodies. Many stony meteorite classes retain the chemical signatures of the complete or partial loss of metallic melts (e.g., Mittlefehldt 2003). Iron meteorites represent samples of separated metallic melts (e.g., McCoy and Haack 2003). In larger planetary bodies, metallic melts also separated from silicates, forming central metallic cores and rocky mantles. During core formation on these bodies, the composition of the metallic melt had an effect on the partitioning of elements between the core and mantle (e.g., Walter et al. 2000). Once a central core was formed, the composition of the metal continued to influence the evolution of that core, as the core began to cool and solidify and elements were distributed between solid and liquid portions (e.g., Brandon et al. 2003; Chabot and Haack 2006).

Experimental studies have shown that the composition of a metallic melt can have a significant effect on the partitioning behavior of elements (Willis and Goldstein 1982; Jones and Drake 1983). In the Fe-S system, the solid metal/liquid metal partitioning value for Ir increases by about three orders of magnitude from the S-free system to a composition near

the Fe-FeS eutectic (Jones and Drake 1983). In contrast, some elements, such as Cu, exhibit chalcophile (S-loving) tendencies and have decreasing solid metal/liquid metal values with increasing S content of the metallic melt (Chabot et al. 2009). Thus, not only does the presence of S in the metallic melt influence the partitioning behavior of elements but it also affects different elements in fundamentally different ways.

Along with S, other nonmetals and metalloids have been discussed as important components of metallic melts in planetary systems. Phosphorus in iron meteorites is suggested to have been at high enough levels to cause liquid immiscibility in the Fe-S-P system for some iron meteorite groups (Ulff-Møller 1998). Earth's outer core is substantially less dense than pure Fe-Ni, requiring about 3–9% of the core to be composed of nonmetals and/or metalloids (Anderson and Isaak 2002). Taking into account their cosmochemical availability, the elements H, C, O, and Si, along with S, have been proposed as significant nonmetals and metalloid in Earth's core (Hillgren et al. 2000).

Previous studies have examined the effects of S (Chabot et al. 2003, 2009), P (Corrigan et al. 2009), and C (Chabot et al. 2006) on the partitioning behavior of numerous trace elements. However, similar studies for the elements of H, O, and Si have not been conducted, due mainly to the different phase relationships of these nonmetals and metalloid with Fe. Solid metal/liquid metal studies in the Fe-S, Fe-P, and Fe-C systems have all taken advantage of the eutectic present in the Fe-rich portion of these systems and that these nonmetals are not soluble in solid Fe metal above the level of a few weight percent (Massalski 1990). Similar simple solid metal/liquid metal studies in the Fe-Si, Fe-O, and Fe-H systems are not possible because of the different phase relations in these systems. To explore the effects of these important metalloid and nonmetals, a different approach must be used.

The goal of this study is to explore the effect of Si in Fe-bearing metallic melts on trace element partitioning behavior. Solid metal/liquid metal experiments in the Fe-Si system are not well-suited for this goal because significant amounts of Si are soluble in solid Fe metal, resulting in very little difference in the Si content of coexisting solid metal and liquid metal in the Fe-Si system (Massalski 1990). Experiments with coexisting metal and silicate could be conducted with varying amounts of Si in the metallic phase. However, varying the Si content of the metal would also result in significant variations in the oxygen fugacity from experiment to experiment (Wade and Wood 2005), complicating the determination of compositional versus oxygen fugacity effects. Thus, we decided to conduct experiments with two coexisting metallic liquids in the Fe-S-Si system. Conducting experiments in the Fe-S-Si system allows us to leverage the extensive available knowledge about the effect of S (Chabot et al. 2003, 2009) while exploring the effect of Si. New results for 22 trace elements are presented and discussed.

EXPERIMENTAL AND ANALYTICAL METHODS

At 0.1 MPa, there is a large liquid immiscibility field in the Fe-S-Si system (Raghavan 1988). Experiments conducted with bulk compositions that fall within the liquid immiscibility field result in two metallic liquids: one S-rich and one Si-rich. The bulk composition and the temperature will dictate the compositions of the coexisting immiscible metallic liquids. A temperature of 1400 °C was chosen for our study. At 1400 °C, for low bulk S and Si contents, solid Fe-Si alloy can coexist with a single S and Si-bearing metallic liquid, though the compositional differences between the solid and the liquid will be small. At 1400 °C and slightly higher S and Si contents, there is a small region where a single metallic liquid will exist without any solid metal phase. For the majority of S and Si bulk contents at 1400 °C, the composition will fall in the large two-liquid immiscibility field, and the bulk compositions of our experiments were selected accordingly to produce two immiscible liquids. Our study temperature of 1400 °C is too high for solid Fe-Si alloy to coexist with two liquids; the highest temperature at which these three phases coexist in the Fe-S-Si system is 1330 °C.

All experiments were conducted at 0.1 MPa and 1400 °C in a Deltech vertical tube furnace at the Johns Hopkins University Applied Physics Laboratory, using similar techniques to previous studies conducted in this lab (Chabot et al. 2007, 2009). Starting powders of Fe, FeS, and Si, with 22 trace elements doped at about approximately 100 ppm each were mixed. At this low level, it is possible to include multiple trace elements in the study with little additional effort and without affecting the partitioning behaviors (e.g., Chabot et al. 2003, 2007). The trace elements included Ag, As, Au, Co, Cr, Cu, Ga, Ge, Ir, Mo, Ni, Os, Pd, Pt, Re, Rh, Ru, Sb, Sn, V, W, and Zn. About 200 mg of a starting power was placed directly in a high purity silica tube. The tube was then evacuated, sealed, and hung in the furnace for durations of approximately 20 h. At a temperature of 1250 °C, Malvin et al. (1986) conducted a time series study, demonstrating that similar solid metal/liquid metal trace element partitioning behavior was achieved for experiments that were conducted for durations of 21 days to just 5 h. Since our experiments involve two liquids and a temperature of 1400 °C,

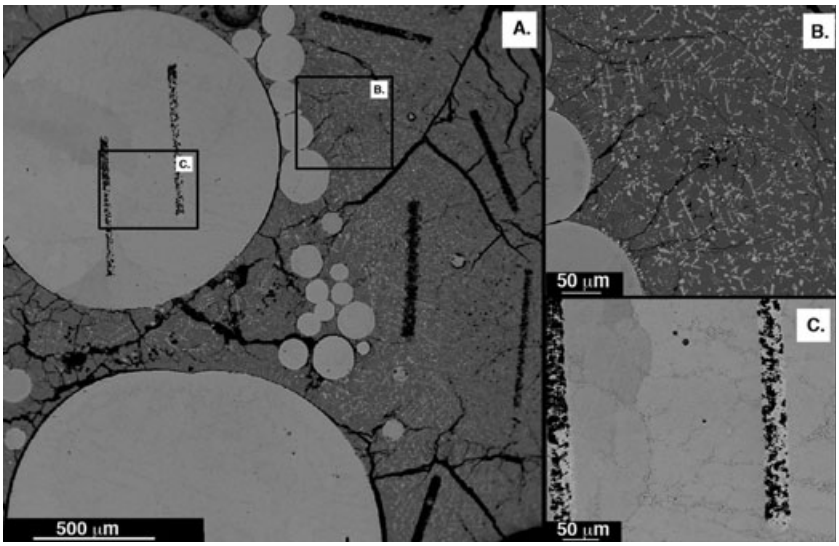

Fig. 1. Back-scattered electron (BSE) images of experiment #TS5. a) Run products contained two quenched immiscible metallic liquids, one S-rich and one Si-rich. The dark lines were produced during laser ablation ICP-MS microanalysis. b) The S-rich liquid exhibits a distinct quench texture, with Fe dendrites surrounded by interstitial FeS. c) The Si-rich liquid also shows a quench texture but the texture is much more subtle, likely due to the higher solubility of Si than S in solid Fe metal.

durations of approximately 20 h are sufficient to reach equilibrium partitioning behavior. Though the starting powders were placed directly in high purity SiO_2 glass tubes, the final run products showed no significant interaction with the silica tubes. Rather, run products were easily removed from the tubes following the completion of the experiment and often rolled easily out of the tubes as small metal balls. Run products were mounted in epoxy, sliced with a diamond saw, and polished for inspection and analysis.

Run products were first inspected and analyzed using the JEOL 8900L electron microprobe at the Carnegie Institution of Washington. As shown in the back-scattered electron (BSE) images of Fig. 1, run products consisted of two clearly distinguished immiscible metallic liquids. Both liquids exhibited quench textures. Figure 1b shows the typical dendritic quench texture of a S-rich liquid, with Fe dendrites surrounded by interstitial FeS. The quench texture of the Si-rich liquid is also present but significantly less pronounced, as shown in Fig. 1c, likely due to the much greater solubility of Si in solid Fe metal as compared to S. Major elements of Fe, S, and Si were analyzed using electron microprobe settings of 15 kV, 30 nA, counting times of 30 s, and a raster beam size of 10×10 μm^2. Between 30 and 50 measurements were averaged to determine the composition of each liquid, and errors were calculated as twice the standard deviation of the mean. Using image processing and analysis techniques, Chabot and Drake (1997) demonstrated that this analysis approach produces reliable bulk compositions for Fe-S liquids with similar dendritic quench textures. Concentrations of O were also roughly estimated at the same time with the same conditions on the electron microprobe. We did not establish a robust calibration method for O, and the examination of O with the electron microprobe was meant to verify that experiments had not oxidized to any significant amount during the run rather than to obtain accurate measurements of O contents. Some experiments did show significant (>1 wt%) concentrations of O or metallic liquid compositions that were inconsistent with the Fe-S-Si phase diagram (Raghavan 1988) and were consequently discarded from further analysis.

In total, seven experiments with coexisting S-rich and Si-rich immiscible liquids were successfully conducted with a range of resulting liquid compositions. Table 1 lists the compositions of the liquids in the seven experiments. Probe data reported on Table 1 were all collected during the same probe session, for further consistency and comparisons between experiments. Figure 2 plots the compositions of the liquids and shows that there is very good agreement between the compositions of the experiments and the published Fe-S-Si phase diagram (Raghavan 1988).

Laser ablation inductively coupled plasma mass spectrometry (ICP-MS) microanalysis at the University of Maryland was conducted to measure trace element concentrations. Analyses were conducted using a single-collector ICP-MS (Element 2, Thermo Electron Corp) coupled to a laser ablation system with an output wavelength at 213 nm (UP213, New Wave Research).

Table 1. Run conditions and compositions of experimental run products.

Run number	TS18	TS5	TS9	TS17	TS22	TS10	TS1
Duration (h)	21	21	26.5	20.5	24	17	20.5
Temp (°C)	1400	1400	1400	1400	1400	1400	1400
Sulfur liquid							
Fe (wt%)	69.7 ± 1.2	69.1 ± 1.0	69.0 ± 0.9	67.2 ± 0.8	66.8 ± 1.0	65.5 ± 0.6	64.8 ± 0.6
S (wt%)	29.6 ± 1.3	30.0 ± 0.9	29.7 ± 0.8	31.5 ± 0.8	31.9 ± 0.7	33.4 ± 0.6	34.2 ± 0.6
Si (wt%)	0.12 ± 0.03	0.07 ± 0.02	0.3 ± 0.3	0.3 ± 0.3	0.3 ± 0.3	0.1 ± 0.2	0.03 ± 0.01
Ag (ppm)	78 ± 9	130 ± 20	220 ± 30	99.5 ± 0.5	210 ± 40	220 ± 30	270 ± 60
As (ppm)	34 ± 2	67 ± 7	31 ± 3	26 ± 2	47 ± 5	30 ± 2	61 ± 6
Au (ppm)	40.4 ± 0.9	270 ± 30	75 ± 11	73 ± 9	50 ± 3	126 ± 6	200 ± 40
Co (ppm)	40.9 ± 1.5	84 ± 7	40 ± 2	26 ± 2	53 ± 3	19.8 ± 1.3	38 ± 5
Cr (ppm)	234 ± 12	254 ± 15	330 ± 30	290 ± 20	310 ± 50	340 ± 20	470 ± 70
Cu (ppm)	410 ± 20	770 ± 40	600 ± 50	550 ± 20	879 ± 80	980 ± 30	1190 ± 150
Ga (ppm)	11.2 ± 0.7	26 ± 5	10.3 ± 0.7	9.4 ± 1.2	16 ± 4	18 ± 4	35 ± 7
Ge (ppm)	15 ± 2	26 ± 5	9 ± 2	6.5 ± 0.8	9 ± 2	6.2 ± 1.2	13 ± 3
Ir (ppm)	1.3 ± 0.3	0.73 ± 0.13	0.14 ± 0.04	0.12 ± 0.03	–	–	0.011 ± 0.003
Mo (ppm)	42 ± 2	112 ± 8	18.1 ± 0.9	22.9 ± 0.9	23 ± 2	26 ± 2	36 ± 5
Ni (ppm)	174 ± 8	102 ± 5	44 ± 4	114 ± 5	176 ± 12	72 ± 4	25 ± 5
Os (ppm)	–	0.28 ± 0.06	0.09 ± 0.02	0.05 ± 0.01	–	–	0.009 ± 0.003
Pd (ppm)	20.5 ± 1.4	59 ± 7	23 ± 2	16 ± 2	22 ± 2	13.1 ± 0.7	26 ± 7
Pt (ppm)	4.2 ± 0.6	8 ± 2	1.12 ± 0.13	1.13 ± 0.17	0.5 ± 0.2	–	0.34 ± 0.06
Re (ppm)	0.6 ± 0.2	0.33 ± 0.08	0.09 ± 0.03	0.025 ± 0.006	–	–	0.017 ± 0.001
Rh (ppm)	6.9 ± 0.7	11 ± 1	0.82 ± 0.10	2.4 ± 0.4	0.9 ± 0.3	0.8 ± 0.3	0.16 ± 0.02
Ru (ppm)	4.9 ± 0.6	10 ± 2	1.1 ± 0.2	1.15 ± 0.13	0.5 ± 0.3	–	0.22 ± 0.03
Sb (ppm)	108 ± 5	260 ± 20	210 ± 20	146 ± 7	230 ± 30	360 ± 18	340 ± 40
Sn (ppm)	99 ± 6	210 ± 20	141 ± 12	109 ± 3	250 ± 30	490 ± 60	490 ± 140
V (ppm)	148 ± 8	230 ± 10	143 ± 11	300 ± 20	500 ± 100	780 ± 80	330 ± 80
W (ppm)	1.4 ± 0.3	2.7 ± 0.5	0.51 ± 0.06	0.30 ± 0.01	0.30 ± 0.13	0.36 ± 0.14	1.02 ± 0.07
Zn (ppm)	202 ± 2	290 ± 9	137 ± 6	340 ± 30	641 ± 33	980 ± 30	540 ± 30
Total (wt%)	100.0	99.5	99.4	99.6	99.5	99.4	99.4
Silicon liquid							
Fe (wt%)	90.4 ± 1.0	91.4 ± 0.1	91.2 ± 0.1	90.3 ± 0.2	89.2 ± 0.2	86.9 ± 0.1	86.3 ± 0.2
S (wt%)	4.3 ± 1.1	2.1 ± 0.1	1.9 ± 0.1	2.4 ± 0.4	1.2 ± 0.1	0.7 ± 0.1	0.6 ± 0.1
Si (wt%)	4.9 ± 0.2	6.4 ± 0.1	7.4 ± 0.1	7.6 ± 0.1	9.7 ± 0.1	13.2 ± 0.1	13.1 ± 0.2
Ag (ppm)	2.5 ± 0.9	2.1 ± 0.3	2.4 ± 0.3	3.2 ± 0.9	1.28 ± 0.02	1.4 ± 0.4	4.0 ± 0.9
As (ppm)	80 ± 2	191 ± 5	79.4 ± 1.2	78 ± 4	140 ± 10	89 ± 3	214 ± 16
Au (ppm)	87.8 ± 1.3	750 ± 60	206 ± 4	216 ± 7	161 ± 6	418 ± 8	750 ± 20
Co (ppm)	122.1 ± 1.3	323.3 ± 0.9	135.7 ± 0.6	108 ± 3	247 ± 2	118 ± 2	280 ± 10
Cr (ppm)	37 ± 8	23.7 ± 0.9	35 ± 2	42 ± 2	22 ± 2	23 ± 3	26 ± 7
Cu (ppm)	111 ± 13	153 ± 7	129 ± 4	163 ± 6	140 ± 10	145 ± 18	180 ± 40
Ga (ppm)	53 ± 2	151 ± 4	56 ± 2	51 ± 2	93 ± 4	49 ± 3	8.0 ± 0.4
Ge (ppm)	123 ± 6	347 ± 6	105 ± 4	115 ± 3	216 ± 13	125 ± 3	274 ± 11
Ir (ppm)	143 ± 12	494 ± 4	106 ± 3	114 ± 5	–	–	246 ± 9
Mo (ppm)	282 ± 9	898 ± 7	175.7 ± 1.4	241 ± 6	290 ± 20	369 ± 8	439 ± 6
Ni (ppm)	332 ± 6	240 ± 10	94 ± 7	294 ± 8	500 ± 20	282 ± 18	111 ± 3
Os (ppm)	–	394 ± 4	74 ± 2	79 ± 4	–	–	197 ± 8
Pd (ppm)	53 ± 4	198 ± 7	68.1 ± 1.1	66.2 ± 0.9	108 ± 6	82 ± 4	190 ± 7
Pt (ppm)	140 ± 10	646 ± 6	118 ± 3	128 ± 5	162 ± 4	–	266 ± 13
Re (ppm)	130 ± 10	385 ± 6	76.5 ± 1.4	41.9 ± 1.2	–	–	209 ± 9
Rh (ppm)	159 ± 11	520 ± 20	51.1 ± 0.4	182 ± 3	170 ± 10	340 ± 9	126 ± 2
Ru (ppm)	216 ± 14	1150 ± 40	157 ± 3	227 ± 6	242 ± 16	–	411 ± 5
Sb (ppm)	75 ± 5	179 ± 4	118 ± 5	136 ± 7	114 ± 4	150 ± 20	193 ± 9
Sn (ppm)	108 ± 5	231 ± 8	119 ± 6	139 ± 7	150 ± 7	157 ± 10	137 ± 12
V (ppm)	23 ± 5	20.7 ± 0.9	15 ± 1	44.6 ± 1.3	32 ± 4	48 ± 8	17 ± 5
W (ppm)	50 ± 2	292 ± 5	60.1 ± 1.0	37 ± 2	64 ± 3	65.7 ± 1.0	156 ± 10
Zn (ppm)	45 ± 7	40.2 ± 1.1	20 ± 2	66 ± 7	43 ± 5	35 ± 8	17 ± 5
Total (wt%)	99.8	100.1	100.6	100.5	100.2	101.0	100.2

Errors are ±2 standard deviations of the mean.

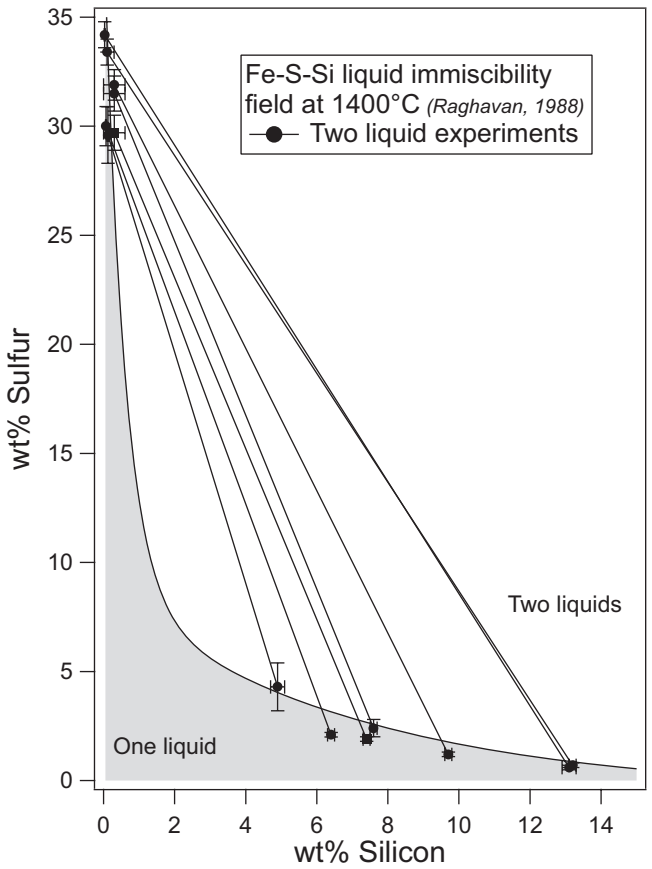

Fig. 2. The S and Si compositions of the two liquids produced in the experiments show good agreement with the published Fe-S-Si liquid immiscibility field at 1400 °C (Raghavan 1988). The coexisting liquids in each experiment are linked with a tie line and plotted with two sigma error bars.

The laser was operated at approximately 1.5 J cm^{-2}. Ablation sampling was done in line scan mode using a 65 μm diameter spot and 10 Hz flash rate for the S-rich liquid and a 40 μm diameter spot and 10 Hz flash rate for the Si-rich liquid. During ablation, the sample was moved at a rate of 10 μm s^{-1}. The length of each line varied depending on the characteristics of each experimental sample, but the length was generally between 500 and 800 μm. At least four line scans were conducted in each of the two liquid phases. The BSE images in Fig. 1 show the linear scars left on an experimental run product due to the laser ablation ICP-MS analysis techniques. This analysis approach has been proven to be effective for measuring the compositions of similar Fe-bearing metallic experimental samples with liquid metal present (Chabot et al. 2007, 2009).

During analysis, data were collected for the following masses: ^{51}V, ^{53}Cr, ^{57}Fe, ^{59}Co, ^{62}Ni, ^{63}Cu, ^{65}Cu, ^{66}Zn, ^{67}Zn, ^{69}Ga, ^{71}Ga, ^{72}Ge, ^{73}Ge, ^{75}As, ^{95}Mo, ^{97}Mo, ^{99}Ru, ^{101}Ru, ^{103}Rh, ^{105}Pd, ^{107}Ag, ^{108}Pd, ^{109}Ag, ^{117}Sn, ^{118}Sn, ^{121}Sb, ^{123}Sb, ^{182}W, ^{183}W, ^{185}Re, ^{188}Os, ^{189}Os, ^{191}Ir, ^{193}Ir, ^{194}Pt, ^{195}Pt, and ^{197}Au. Analyses of two standard reference materials were conducted both before and after the analyses of the experimental run products: NIST 610 (Jochum and Stoll 2008) with a 55 μm spot size and North Chile (Filomena) (electronic annex of Walker et al. 2008) with a 40 μm spot size. These standard reference materials provided the basis for determining calibration curves to constrain instrument drift and provide element concentrations. Element concentrations for Ag, As, Co, Cr, Cu, Ga, Ge, Mo, Ni, Sb, Sn, V, and Zn were standardized using the NIST 610 standard. Element concentrations for Au, Ir, Os, Pd, Pt, Re, Rh, Ru, and W were standardized using the North Chile (Filomena) standard. Data were processed using the LAMTRACE (Achterbergh et al. 2001) software program, which determines element concentrations using ratios of count rates for samples and standards, known concentrations in the standards, and the known concentration of an internal standard in the experimental run products. Errors in the composition of each phase were calculated as twice the standard error of the mean. Table 1 lists the concentrations measured for each trace element in the S-rich and Si-rich liquids. Measurements below the detection limit, defined as background plus three standard deviations of the background, or measurements where the standard error of the mean was greater than 33% are not reported in Table 1.

PARTITIONING RESULTS

Table 2 lists the calculated Si liquid/S liquid $D_{Si/S}$ ratios for the trace elements in the seven experiments. The Si liquid/S liquid $D_{Si/S}$ values were calculated as:

$$D_{Si/S}(E) = \frac{\text{wt\%}E(\text{Si liquid})}{\text{wt\%}E(\text{S liquid})} \quad (1)$$

Errors in Table 2 were calculated by using the two standard deviation of the mean errors for both liquids reported in Table 1 and assuming that errors in the Si liquid and in the S liquid were independent.

The partitioning behaviors of trace elements in these Fe-S-Si experiments are being affected by both the S-rich liquid and Si-rich liquid that coexisted in the runs. Our first step was thus to compare our newly measured $D_{Si/S}$ values to previously determined solid metal/S liquid $D_{met/S}$ values. Figures 3a and 3c show this comparison for Ni and Co. Solid metal/S liquid $D_{met/S}$ data from partitioning in the Fe-S system are plotted as a function of the S content of the metallic

Table 2. Partition coefficients from experiments, $D_{Si/S}$.

Run number	TS18	TS5	TS9	TS17	TS22	TS10	TS1
Duration (h)	21	21	26.5	20.5	24	17	20.5
Temp (°C)	1400	1400	1400	1400	1400	1400	1400
$D_{Si/S}$							
Ag	0.03 ± 0.01	0.017 ± 0.003	0.019 ± 0.003	0.03 ± 0.01	0.006 ± 0.001	0.006 ± 0.002	0.02 ± 0.01
As	2.37 ± 0.13	2.8 ± 0.3	3.0 ± 0.3	3.1 ± 0.3	3.0 ± 0.4	2.9 ± 0.2	3.5 ± 0.5
Au	2.17 ± 0.06	2.78 ± 0.12	3.1 ± 0.4	3.0 ± 0.4	3.2 ± 0.2	3.31 ± 0.16	3.8 ± 0.7
Co	2.99 ± 0.11	3.9 ± 0.3	3.8 ± 0.2	4.2 ± 0.3	4.7 ± 0.2	5.9 ± 0.4	7.4 ± 1.0
Cr	0.16 ± 0.03	0.09 ± 0.01	0.11 ± 0.01	0.14 ± 0.01	0.07 ± 0.01	0.07 ± 0.01	0.06 ± 0.02
Cu	0.27 ± 0.04	0.20 ± 0.01	0.21 ± 0.02	0.30 ± 0.02	0.16 ± 0.02	0.15 ± 0.02	0.15 ± 0.04
Ga	4.7 ± 0.3	5.7 ± 1.1	7.9 ± 0.6	5.4 ± 0.7	5.7 ± 1.3	2.7 ± 0.7	3.6 ± 0.9
Ge	8.2 ± 0.9	13 ± 2	17 ± 4	18 ± 2	23 ± 6	19 ± 4	20 ± 4
Ir	110 ± 30	700 ± 100	1300 ± 300	900 ± 300	–	–	22000 ± 6000
Mo	6.8 ± 0.4	8.0 ± 0.6	10.5 ± 0.5	10.5 ± 0.5	12.5 ± 1.4	14.1 ± 1.2	12 ± 2
Ni	1.91 ± 0.09	2.33 ± 0.15	2.1 ± 0.2	2.59 ± 0.14	2.9 ± 0.2	3.9 ± 0.3	4.5 ± 0.9
Os	–	1400 ± 300	2100 ± 500	1600 ± 400	–	–	22000 ± 7000
Pd	2.6 ± 0.3	3.3 ± 0.4	3.1 ± 0.3	4.1 ± 0.6	4.9 ± 0.6	6.3 ± 0.5	7.2 ± 1.9
Pt	31 ± 5	76 ± 15	190 ± 20	113 ± 18	310 ± 150	–	770 ± 140
Re	110 ± 40	1200 ± 300	1500 ± 500	2000 ± 400	–	–	12000 ± 600
Rh	23 ± 3	48 ± 7	95 ± 12	77 ± 13	190 ± 60	400 ± 200	780 ± 110
Ru	44 ± 6	120 ± 20	260 ± 30	180 ± 40	500 ± 300	–	1900 ± 300
Sb	0.69 ± 0.05	0.69 ± 0.05	0.60 ± 0.07	0.93 ± 0.07	0.49 ± 0.07	0.39 ± 0.05	0.57 ± 0.08
Sn	1.09 ± 0.08	1.11 ± 0.11	0.85 ± 0.09	1.28 ± 0.08	0.61 ± 0.09	0.32 ± 0.05	0.28 ± 0.10
V	0.16 ± 0.03	0.09 ± 0.01	0.10 ± 0.01	0.15 ± 0.01	0.07 ± 0.02	0.06 ± 0.01	0.05 ± 0.02
W	37 ± 8	110 ± 20	220 ± 20	142 ± 7	200 ± 100	180 ± 70	153 ± 14
Zn	0.22 ± 0.03	0.14 ± 0.01	0.13 ± 0.01	0.19 ± 0.03	0.07 ± 0.01	0.04 ± 0.01	0.03 ± 0.01

Errors are ±2 standard deviations of the mean.

liquid (Chabot et al. 2003, 2009). Our measured $D_{Si/S}$ values are also plotted as a function of the S content of the S-rich metallic liquid. In our experiments, the S-rich liquid has S contents between 29 and 34 wt%, values that just overlap with the highest S content experiments in the Fe-S system and extend to even higher S values. Our $D_{Si/S}$ values for Ni and Co plotted on Figs. 3a and 3c show a similar increasing trend with increasing S content of the metallic liquid as that seen in the previous $D_{met/S}$ data.

Fits to the previous Fe-S $D_{met/S}$ data, parameterized as a function of the S content of the metallic liquid, are also shown on Fig. 3 (Chabot and Jones 2003). To examine the effect of Si, we utilized the Fe-S system $D_{met/S}$ fits to account for the effect of S. The equation of the fit, as discussed in Chabot and Jones (2003) is:

$$\frac{1}{D_{met/S}} = \frac{1}{D_O}\left(\frac{1-2X_S}{1-X_S}\right)^{\beta} \quad (2)$$

where D_O in the solid/liquid partitioning value in the light-element-free system, X_S is the mole fraction of S in the liquid, and β is a constant unique to the element being fit. Table 3 lists the D_O and β values used for the parameterized fits of each element and references to the published $D_{met/S}$ studies in the Fe-S system.

Using the S content for the S-rich liquid reported in Table 1 for each of our seven experiments, we calculate the corresponding $D_{met/S}$ value for each element from Equation 2 and Table 3. Next, we divided this $D_{met/S}$ value from Equation 2 by the measured $D_{Si/S}$ value listed in Table 2. We define this quantity as $D'_{met/Si}$, which is expressed mathematically as:

$$D'_{met/Si} = \frac{D_{met/S}}{D_{Si/S}} \quad (3)$$

This $D'_{met/Si}$ value neglects the effect of Si dissolved in the S-rich metallic liquid, but as seen on Table 1, the S-rich liquid contains <0.3 wt% Si. For Ni and Co, $D'_{met/Si}$ is plotted as a function of the Si content of the Si-rich liquid on Figs. 3b and 3d. Also shown on Figs. 3b and 3d are the solid metal/liquid metal D_O values from the parameterized fits for Ni and Co for the S-free system, which would be expected to be the same as the Si-free values. The same parameterized fits for the S-bearing system as shown in Figs. 3a and 3c are also plotted on Figs. 3b and 3d for comparison.

Thus, Figs. 3b and 3d show the effect on Ni and Co partitioning behavior due to different amounts of Si in the metallic liquid. For both elements, the partitioning behavior appears largely indifferent to the amount of Si in the metallic liquid. For a range of Si

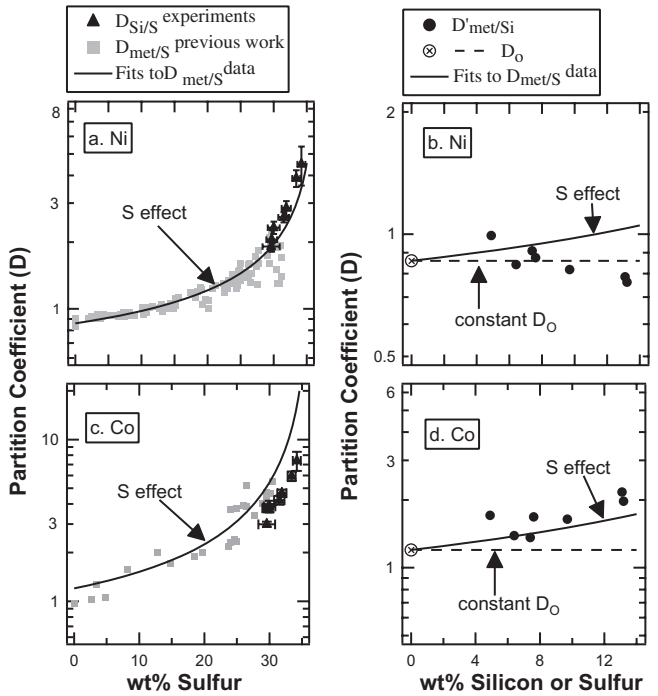

Fig. 3. Results for Ni and Co, illustrating the data analysis approach. Newly measured values of $D_{Si/S}$ from the experiments are compared to published $D_{met/S}$ values and fits to that previous data. By dividing the $D_{met/S}$ fits by the measured $D_{Si/S}$ values, calculated $D'_{met/S}$ values can be determined. These $D'_{met/S}$ values are plotted against the Si content of the Si-rich metallic melt to explore the effect of Si on trace element partitioning behavior. Results are shown for (a and b) Ni and (c and d) Co. References for the previous $D_{met/S}$ data are compiled in Chabot et al. (2003, 2009), and Table 3 lists the parameters of the fits, including the D_O values for the nonmetal free system.

Table 3. Parameterization values for the Fe-S system.

Element	D_O	β (Fe domains)	Reference
As	0.25	1.9	2
Au	0.27	2.1	2
Co	1.2	1.1	2
Ga	0.78	2.6	1
Ge	0.66	3.0	1
Ir	1.5	4.9	1
Mo	0.9	1.1	2
Ni	0.86	0.6	1
Os	2.0	5.1	1
Pd	0.43	1.1	1
Pt	0.81	4.4	1
Re	2.0	5.0	1
Rh	2.6	2.1	2
Ru	2.6	3.4	2
Sb	0.05	1.5	2
Sn	0.10	1.1	2
W	1.2	3.6	1

Element	D_O	D_S	β (FeS domains)	Reference
Ag	0.3	0.0036	1.4	This work
Cr	0.8	0.097	0.75	This work
Cu	0.8	0.16	0.41	2
V	0.4	0.022	0.91	This work
Zn	0.3	0.24	0.068	This work

References: 1. Chabot and Jones 2003; 2. Chabot et al. 2009.

contents from 0 to 13 wt%, Ni and Co show less than a factor of two change in their behavior. This suggests that Ni and Co would partition similarly between a Si-free liquid and a 13 wt% Si-rich liquid. This behavior is also generally comparable to the behavior of Ni and Co over the same range of S contents of 0 to 13 wt%. In fact, Fig. 3d shows good agreement between our calculated $D'_{met/Si}$ value for Co and the parameterized fit from the solid metal-S liquid system. Figure 3b shows a hint of Si-loving behavior for Ni, but any trend is well within the uncertainties in our method for calculating the $D'_{met/Si}$ values, which are discussed in more detail later.

The same approach just discussed for Ni and Co was applied to 20 additional trace elements contained in our experiments, to explore the effect of Si in the metallic liquid on the partitioning behaviors. Results for 15 of those trace elements that exhibit siderophile behavior in the Fe-S system are shown on the two parts of Fig. 4. The first part of Fig. 4 plots the $D_{Si/S}$ values measured directly from our experiments in comparison to previously determined $D_{met/S}$ values in the Fe-S system. The second part of Fig. 4 displays $D'_{met/Si}$ values determined using Equation 3 and enables the effect of Si to be examined.

In contrast to the behavior of Ni and Co, some trace elements show strong changes in their partitioning behaviors due to the presence of Si in the metallic liquid. For example, the data for Ga in Fig. 4r show about a two order of magnitude change for Ga partitioning between a Si-free liquid and a liquid with 13 wt% Si. As the Si content of the metallic liquid increases, Ga partitions less into the liquid. This effect of Si on Ga partitioning behavior is similar in nature to the effect of S on Ga partitioning behavior but considerably larger in magnitude when the same S and Si contents are compared, as seen on Fig. 4r. Other elements, such as As, Au, Ge, Sb, and Sn show similar partitioning behaviors, with avoidance of both S and Si in metallic liquids but a much stronger avoidance of Si than S for any given light element concentration level.

Figure 5 shows results for the four chalcophile elements measured in our experiments (Ag, Cr, Cu, and V) as well as the element Zn, which exhibits a trace of chalcophile tendencies in the Fe-S system. The

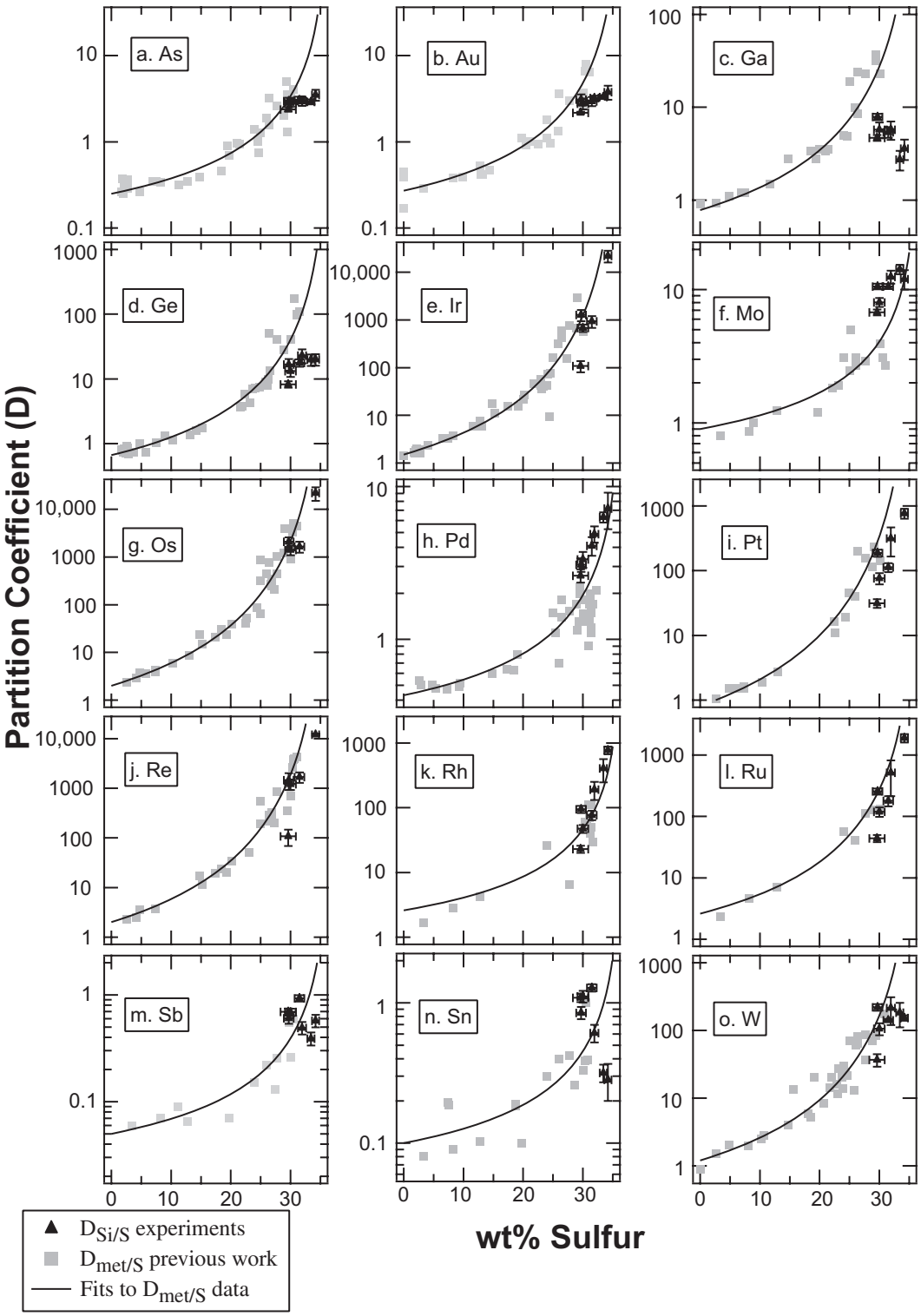

Fig. 4. Results for 15 trace elements that exhibit siderophile behavior in the Fe-S system. In the first part of this figure, measured values of $D_{Si/S}$ from our experiments are compared to published $D_{met/S}$ values and fits to that previous data. In the second part of this figure, calculated $D'_{met/Si}$ values are plotted against the Si content of the Si-rich metallic melt to explore the effect of Si on trace element partitioning behavior and compare that effect to fits showing the effect of S. The 15 trace elements on this figure are: a) p) As, b) q) Au, c) r) Ga, d) s) Ge, e) t) Ir, f) u) Mo, g) v) Os, h) w) Pd, i) x) Pt, j) y) Re, k) z) Rh, l) aa) Ru, m) bb) Sb, n) cc) Sn, and o) dd) W. References for the previous $D_{met/S}$ data are compiled in Chabot et al. (2003, 2009), and Table 3 lists the parameters of the fits, including the D_O values for the nonmetal free system.

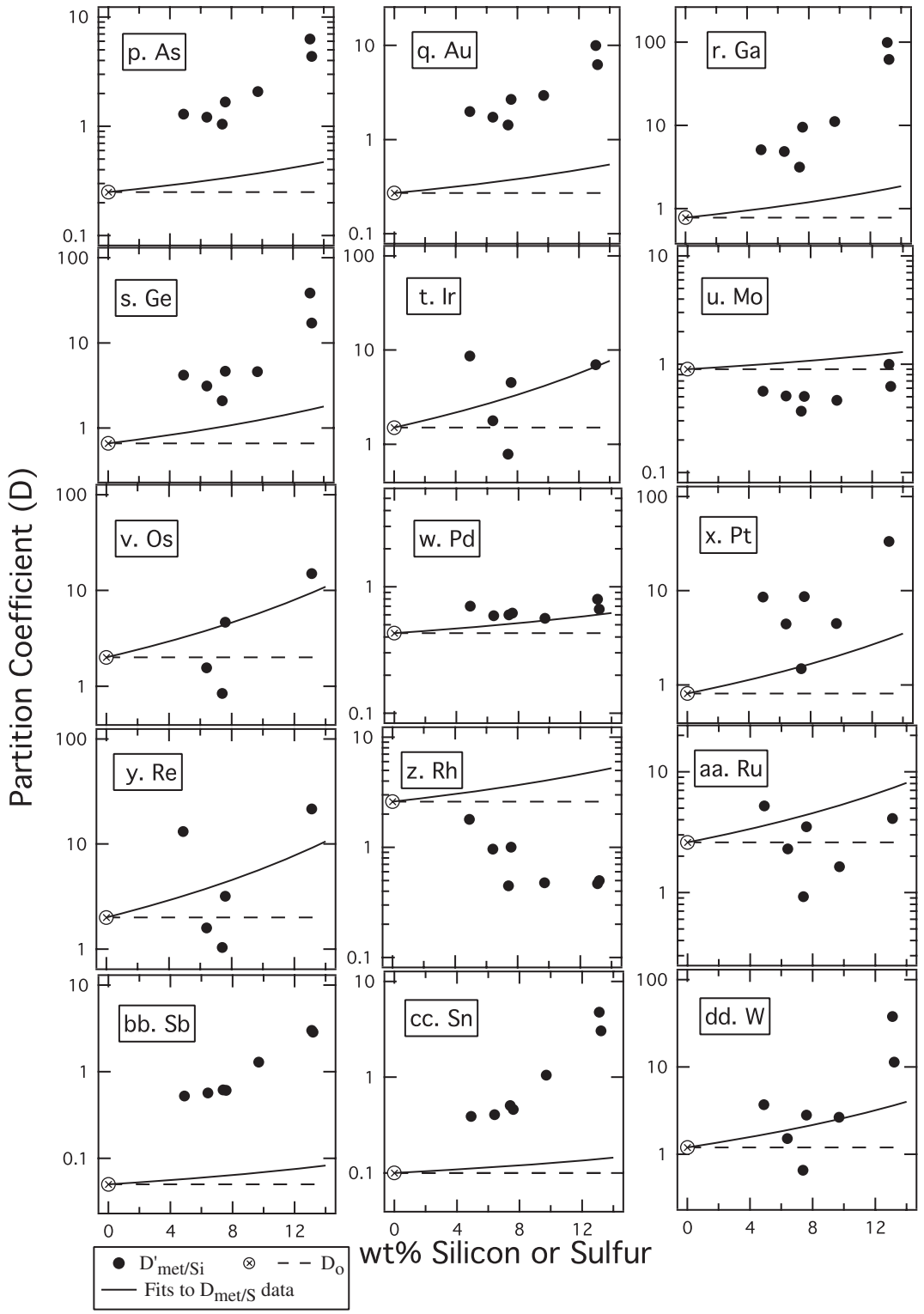

Fig. 4. *Continued.* Results for 15 trace elements that exhibit siderophile behavior in the Fe-S system. In the first part of this figure, measured values of $D_{Si/S}$ from our experiments are compared to published $D_{met/S}$ values and fits to that previous data. In the second part of this figure, calculated $D'_{met/Si}$ values are plotted against the Si content of the Si-rich metallic melt to explore the effect of Si on trace element partitioning behavior and compare that effect to fits showing the effect of S. The 15 trace elements on this figure are: a) p) As, b) q) Au, c) r) Ga, d) s) Ge, e) t) Ir, f) u) Mo, g) v) Os, h) w) Pd, i) x) Pt, j) y) Re, k) z) Rh, l) aa) Ru, m) bb) Sb, n) cc) Sn, and o) dd) W. References for the previous $D_{met/S}$ data are compiled in Chabot et al. (2003, 2009), and Table 3 lists the parameters of the fits, including the D_O values for the nonmetal free system.

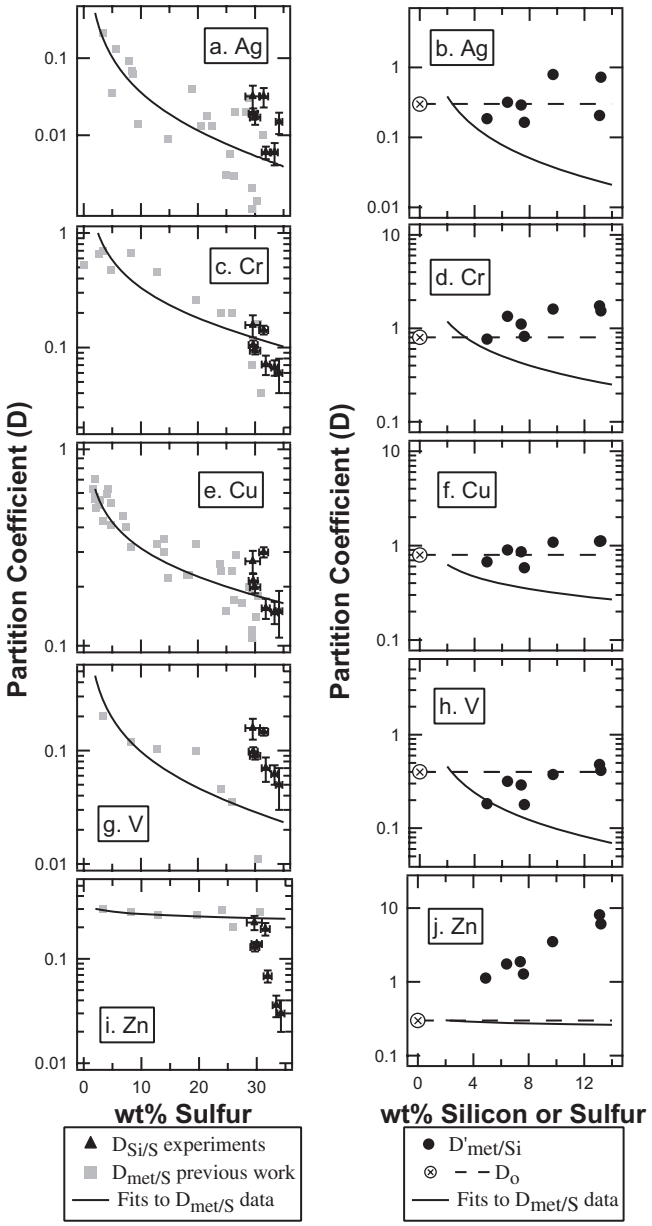

Fig. 5. Results for four chalcophile elements and Zn. Measured values of $D_{Si/S}$ from the experiments are compared to previously determined $D_{met/S}$ values and fits to that previous data. By dividing the fit of $D_{met/S}$ by the measured $D_{Si/S}$ values, calculated $D'_{met/Si}$ values can be determined. These calculated $D_{met/Si}$ values are plotted against the Si content of the Si-rich metallic melt to explore the effect of Si on trace element partitioning behavior. Results are shown for four elements with chalcophile behavior in the Fe-S system and Zn: a and b) Ag, c and d) Cr, e and f) Cu, g and h) V, and i and j) Zn. References for the previous $D_{met/S}$ data are compiled in Chabot et al. (2003, 2009), and Table 3 lists the parameters of the fits and the estimated D_O values for the nonmetal free system.

parameterization method of Chabot and Jones (2003), given in Equation 2, is not appropriate for the parameterization of chalcophile elements, as they show a preference for the S-bearing liquid instead of avoidance. Chabot et al. (2009) introduced an alternate equation for parameterizing chalcophile elements:

$$\frac{1}{D_{met/S}} = \frac{1}{D_S}\left(\frac{X_S}{1 - X_S}\right)^{\beta} \quad (4)$$

where D_S is the solid metal/liquid metal partition coefficient with a liquid composition of FeS, X_S is the mole fraction of S in the metallic liquid, and β is a constant specific to the element being parameterized. Equation 4 becomes undefined when X_S is zero, so parameterized fits from Equation 4 should not be used at low S content values. Thus, solid/liquid D values for the light element free system (D_O) for the five elements plotted on Fig. 5 were estimated from the experimental data. Table 3 lists the parameterized D_S and β values for these elements, as well as estimated D_O values, based on published experiments in the Fe-S system.

In contrast to their S-loving behavior, the presence of Si in the metallic liquid seems to have little effect on the behavior of Ag, Cr, Cu, or V, as shown in Fig. 5. For Zn, the S content of the metallic liquid has little effect on its partitioning behavior but Zn shows a clear avoidance of Si on Fig. 5, partitioning less into the metallic liquid as the Si content increases.

The calculated $D'_{met/Si}$ values plotted in Figs. 3–5 are a way to examine the effects of Si on partitioning behavior and make comparisons between different trace elements. The calculations do contain uncertainties that should be kept in mind. First, the calculation depends on using the measured S content of the S-rich liquid in the experiment to determine the appropriate $D_{met/S}$ value from the parameterization. Thus, any inaccuracy in the measured S content will produce inaccuracy in the $D_{met/S}$ value used to account for the effect of S for that experimental data point.

Second, the calculation depends on the parameterized expression used to determine a $D_{met/S}$ value. The parameterizations are based on fits to published solid metal/liquid metal experiments in the Fe-S system. The previous Fe-S experimental data sets are generally well-sampled for each element, even extensive in some cases with Ni being the extreme, but the Fe-S solid metal/liquid metal partitioning data can only extend up to the Fe-FeS eutectic composition of about 31 wt% S. Four of our seven Fe-S-Si two liquids experiments reported in Table 1 contain >31 wt% S in the S-rich liquid. Thus, the parameterizations developed from experiments in the Fe-S system must be extrapolated to slightly higher S contents of up to 34 wt% S to be applied to our experiments. For many elements, as shown in the first part of Fig. 4, the parameterized $D_{met/S}$ values change rapidly in this region

of high S contents. Consequently, uncertainties in the parameterized expressions result in uncertainties in our calculated $D'_{met/Si}$ values. This uncertainty, combined with any uncertainty in the measured S content, results in considerable scatter for the calculated $D'_{met/Si}$ values, especially for elements that seem to have either weak or no effect from Si on their partitioning behaviors.

Third, the calculated $D'_{met/Si}$ values lack direct meaning to a physical system. As discussed, a solid metal/liquid metal experiment conducted in the Fe-Si system would produce a solid with a concentration of Si nearly as high as the coexisting liquid (Massalski 1990). Our calculated solid metal/Si liquid $D'_{met/Si}$ values are derived from using solid metal/S liquid $D_{met/S}$ values from the Fe-S system, where the solid metal has negligible levels of S or any other nonmetal or metalloid. Thus our calculated $D'_{met/Si}$ value is between a nearly pure Fe(-Ni) solid metal and a Si-bearing liquid, a combination that would not exist in equilibrium with each other in nature.

With these limitations in mind, our experimental results enable the general effect of Si in liquid metal on partitioning behavior to be explored. Which elements seem to have strong avoidance of Si? Which elements show a weaker effect? Which elements show no effect of Si in the liquid, and are there any elements that exhibit Si-loving behavior? Our results provide insight into these general behavior questions. Of the 22 trace elements examined in our experimental study, we have divided the effect of Si on partitioning behavior into four broad categories:

1. Strong Si avoidance. As, Au, Ga, Ge, Sb, Sn, Zn. These elements exhibit at least an order of magnitude change in their partitioning behavior as the Si content of the liquid changes from the Si-free system to one with 13 wt% Si. This Si avoidance is much stronger than the S avoidance shown by these elements for the same range of S contents. Other elements (e.g., Cd and In, and perhaps Tl, Pb and Bi) in the same area of the periodic table could be predicted to exhibit this same strong behavior.
2. Weak Si avoidance. Ir, Os, Pt, Re, Ru, W. These elements all show considerable scatter in their calculated $D'_{met/Si}$ values plotted in Fig. 4, but a weak Si avoidance is suggested by the scattered data. The weak Si avoidance is generally consistent with the S avoidance demonstrated by these elements over a comparable range of S contents. The elements Pt and W may show slightly stronger Si avoidance than S avoidance, but this can not be meaningfully evaluated given the scatter in the data.
3. No Si effect. Ag, Co, Cu, Cr, Ni, Pd, V. These elements show generally similar partitioning behavior for a Si-free system and a Si-rich system with 13 wt% Si in the metallic liquid. The slight Si avoidance seen on the Co and Pd graphs is similar to their behaviors in the S-bearing system, with less than a factor of two variation over the range of nonmetal and metalloid contents of 0 to 13 wt%. In the S-bearing system, Ag, Cu, Cr, and V are distinctly chalcophile but exhibit no comparable Si-loving tendencies.
4. Weak Si attraction. Mo, Rh. Our experiments do not show any element with the clearly Si-loving characteristic of partitioning more strongly into the Si-bearing liquid as the Si content of the liquid increases. However, all of the calculated $D'_{met/Si}$ points for Rh in Fig. 4z and all but one for Mo in Fig. 4u fall below the light-element-free D_O value, suggesting that Rh and Mo may be weakly Si-loving. However, inspection of the measured $D_{Si/S}$ values for Rh and Mo on Figs. 4f and 4k shows that the data could also indicate a weak avoidance of Si or no effect of Si if slightly modified parameterized fits were used for the calculations.

We recognize that the above observations concerning element behavior are nonintuitive and defy predictive attributes. This vexing situation is intrinsically worthy of further study from a crystal chemical and band theory perspective.

PLANETARY APPLICATIONS

Using our new results of the effect of Si in a metallic melt on trace element partitioning behavior, we explore two applications to planetary science that may have involved a Si-bearing metallic melt: the separation of metal from silicate during planetary differentiation and the genesis of highly reduced meteorites such as enstatite chondrites.

Metal-Silicate Separation and Planetary Differentiation

As planetary bodies differentiated across the solar system, metal was separated from silicate. Conditions during differentiation dictate the partitioning of elements between metal and silicate phases. These conditions include pressure, temperature, oxygen fugacity, silicate composition, and metallic composition. All of these conditions can influence the metal/silicate partitioning behaviors of elements. Experiments over the last two decades have demonstrated that no one condition is the dominant influence over all the elements (e.g., Righter and Drake 2003). For example, some elements show significant changes in their partitioning behaviors with changing pressure, such as Ni, while other elements are more strongly affected by changing temperature than changing pressure, such as V.

Our new results allow the first examination of the effects on element partitioning that result from a Si-bearing metallic composition. Even though our experiments examine partitioning between two metallic phases, the effect of Si established by our work is expected to be relevant to partitioning in a metal/silicate system. In their solid metal/liquid metal study involving C-bearing compositions, Chabot et al. (2006) demonstrated that the effect of C established for Cr by solid metal/liquid metal studies was in good agreement with the effect of C determined for Cr by metal/silicate experiments (see Fig. 6 Chabot et al. 2006); in both the solid metal/liquid metal and metal/silicate experiments, the presence of about 4 wt% C caused about a factor of 2 change in the partitioning behavior of Cr, with Cr exhibiting anthracophile (C-loving) behavior in both systems. In addition, these Cr solid metal/liquid metal runs were conducted at 0.1 MPa while the metal/silicate experiments to which they were compared were run at 3 GPa; the good agreement further suggests that the effect of C may be largely independent of pressure. Our new results for the effect of Si can be used to explore what sorts of changes in element partitioning behavior would be caused by the presence of a Si-bearing metal during planetary differentiation and melt-silicate separation events.

The availability of samples of Earth's mantle makes it a common focus of many planetary differentiation studies. In particular, many studies have focused on interpreting the signature of four nonvolatile, moderately siderophile elements: Ni, Co, Mo, and W (Li and Agee 1996, 2001; Righter et al. 1997; Righter and Drake 1999; Gessmann and Rubie, 2000; Chabot et al. 2005; Wade and Wood 2005; Kegler et al. 2008; Cottrell et al. 2009). Because these elements are moderately siderophile, they largely partition into the metallic core instead of the silicate mantle yet a measurable concentration does remain in the silicate mantle, at levels considerably elevated relative to the highly siderophile elements. Additionally, the nonvolatile nature of these elements removes the complexity of understanding what portion of the observed depletion in Earth's mantle is due to metal-silicate separation and which portion is due to volatile loss. Recent studies, based on experimental determinations of the behavior of Ni, Co, Mo, and W, have concluded that the concentrations of these moderately siderophile elements in Earth's mantle may have been set by metal-silicate separation in a deep magma ocean or metal-silicate separation in a magma ocean that became more oxidized with time (Li and Agee 1996, 2001; Righter et al. 1997; Righter and Drake 1999; Gessmann and Rubie, 2000; Chabot et al. 2005; Wade and Wood 2005; Cottrell et al. 2009). However, even though Si has been suggested as a possible light element in Earth's core (Hillgren et al. 2000; Lin et al. 2003), these studies have generally not included what effect a Si-bearing metal would have on the partitioning behavior of Ni, Co, Mo, and W for the simple reason that no such information was available. Thus, our new experimental data allow us to examine some interesting questions for the first time, such as: Would having Si in the metal during Earth's differentiation have produced a distinct elemental signature? How would a Si-bearing metal affect the results of recent differentiation models?

Our experimental results for Ni, Co, Mo, and W indicate that the presence of Si in the metallic melt has little effect on the partitioning behavior of these four nonvolatile moderately siderophile elements, albeit at low pressure. Nickel, Co, Mo, and W all partition similarly into a Si-free liquid and one with 10 wt% Si at 0.1 MPa in our experiments. Our results for W show more scatter than those for Ni, Co, or Mo, but with Si contents <10 wt%, as would be a required limitation for the light element content of Earth's core (Anderson and Isaak 2002), W does not show any significant effect of Si on its partitioning behavior.

This conclusion does not mean to imply that having Si in the metal would not have other implications for planetary differentiation. To get a significant amount of Si solubility in a metallic liquid that is in equilibrium with a silicate liquid does provide constraints on the oxygen fugacity of the system, requiring reducing conditions (e.g., Wade and Wood 2005). The metal-silicate partitioning behaviors of Ni, Co, Mo, and W are all significantly affected by the oxygen fugacity of the system. Current models of Earth's differentiation include this important effect of oxygen fugacity, while the effect of Si is generally not a variable in the parameterizations of the metal-silicate partitioning behavior. Our results suggest that the effect of Si in the metal, independent of the oxygen fugacity effect, is minor for Ni, Co, Mo, and W and including this Si effect would not change the model results for Earth's differentiation in a significant way. Our results are from 0.1 MPa experiments, while Earth's differentiation is believed to have involved much higher pressures. However, the effect of Si on these four elements would have to change drastically with pressure to become an important parameter in modeling the behaviors of these four elements during metal-silicate separation.

Though Earth is the focus of many metal-silicate studies, our data are equally applicable to explore how elements would partition during other metal-silicate separation events that involve a Si-bearing metallic melt. Applications to asteroid-sized bodies would also remove the need to extrapolate our 0.1 MPa results to elevated pressures.

Highly Reduced Meteorites

Enstatite chondrites are highly-reduced rocks, and some of the metal in these and similar meteorites contain significant concentrations of Si (e.g., Keil 1989). In addition, perryite is a common accessory phase in enstatite chondrites (e.g., Brearley and Jones 1998; Lin and El Goresy 2002). Thus, the chemical evolution of these meteorites and the partitioning behaviors of elements in this system would have been influenced by having Si in the metal.

Recent measurements of siderophile elements in metal grains of enstatite-rich meteorites have been used to try to unravel the roles of nebular versus parent body processes for the origin of these metals (Humayun et al. 2009; van Niekerk et al. 2009; Lehner et al. 2010). For some of these meteorites, the siderophile element patterns suggest that solid metal/liquid metal partitioning took place during planetary processes such as partial melting and the injection of impacts melts. However, melting experiments involving the enstatite chondrite Indarch revealed that partial melting in this system is very complex (McCoy et al. 1999). McCoy et al. (1999) found five immiscible metallic or sulfide melts present in the total of their experiments, with each of these melts having a different composition: one S-rich, one C-rich, one P-rich, one Si-rich, and one S-rich with significant amounts of commonly lithophile elements. Thus, depending on the temperature and conditions of partial melting, the melts produced could vary considerably in composition. Experiments such as our new Si-bearing ones presented here have demonstrated that trace element partitioning behavior can be very sensitive to the composition of the metallic liquid. Thus, this sensitivity offers the opportunity to distinguish between these different possible melt compositions involved in the petrogenesis of enstatite-rich meteorites.

This study shows that the partitioning behaviors of some elements are strongly affected by the amount of Si in the metallic melt, as shown on Figs. 4 and 5. These elements include As, Au, Ga, Ge, Sb, Sn, and Zn. As trace element concentrations are used to investigate the history of metallic melts in meteorite parent bodies, these elements may provide insight into the role of Si in the system. A comparison of trace element concentrations in meteoritic silicides, such as perryite, to our experimental results could also provide additional information about the partitioning of trace elements in Si-bearing metallic systems under different conditions. Detailed modeling is needed to investigate effects from the possible combinations of light elements that may have played a role in the complex history of these reduced meteorites, but the distinctive effect of Si on these elements, in comparison to the effects of S, P, or C, may have imparted a unique signature on these meteorites if a Si-bearing metallic melt was involved. Also, for metallic melts with multiple nonmetals and metalloids, the appropriate phase diagrams must be considered. Large liquid immiscibility fields exist for Fe-Ni systems with more than one nonmetal and metalloid, and these phase relations place constraints on the compositions of the metallic melts. Additionally, Si is quite soluble in solid Fe metal, and thus a solid metal that coexists with a Si-bearing liquid metal may contain a significant amount of Si. The effect of Si in the solid metal on partitioning behavior has not been investigated.

SUMMARY

Our new results from experiments in the Fe-S-Si system provide the first look at the effect of Si on the partitioning behavior of 22 trace elements. The following general behavior classifications are determined from the results:

1. Strong Si avoidance: As, Au, Ga, Ge, Sb, Sn, Zn.
2. Weak Si avoidance: Ir, Os, Pt, Re, Ru, W.
3. No significant Si effect: Ag, Co, Cu, Cr, Ni, Pd, V.
4. Possible weak Si attraction: Mo, Rh.

The newly determined effect of Si on trace element partitioning behavior has applications to multiple problems in planetary science, two of which were discussed briefly. First, planetary differentiation models are based heavily on understanding the partitioning behaviors of the moderately siderophile elements of Ni, Co, Mo, and W, and our new results suggest that if Si was an important metalloid during this process, the behaviors of these four elements are only minimally affected by the presence of Si in the segregating metal, especially in comparison to effects from oxygen fugacity and other thermodynamic conditions. Second, the metal of reduced enstatite-rich meteorites may suggest a role of a Si-bearing metallic melt during their history, and our results show that elements strongly influenced by the presence of Si (As, Au, Ga, Ge, Sb, Sn, and Zn) may be useful for further investigations aimed at understanding the genesis of reduced meteorites.

Acknowledgments—This work was supported by NASA grant NNX09AG90G to NLC and NNX08AH76G to WFM. NLC appreciates her continued association with the Carnegie Institution of Washington and the use of the JEOL 8900L electron microprobe. A portion of the effort of TMS was supported through the APL high school mentorship program, and we thank Connie Finney for expertly running that program. We

appreciate comments from Munir Humayun and Alex Ruzicka, which improved this manuscript.

Editorial Handling—Dr. Alex Ruzicka

REFERENCES

Achterbergh E. V., Ryan C. G., Jackson S. E., and Griffin W. L. 2001. Appendix 3: Data reduction software for LA-ICP-MS. In *Laser ablation-ICP-MS in the earth sciences*, vol. 29, edited by Sylvester P. Quebec: Mineralogical Association of Canada. Short Course Series, 243 p.

Anderson O. L. and Isaak D. G. 2002. Another look at the core density deficit of Earth's outer core. *Physics of Earth and Planetary Interiors* 131:19–27.

Brandon A. D., Walker R. J., Puchtel I. S., Becker H., Humayun M., and Revillon S. 2003. ^{186}Os-^{187}Os systematics of Gorgona Island komatiites: Implications for early growth of the inner core. *Earth and Planetary Science Letters* 206:411–426.

Brearley A. J. and Jones R. H. 1998. Chondritic meteorites. In *Planetary materials*, edited by Papike J. J. Reviews in Mineralogy, vol. 36. Washington, D.C.: Mineralogical Society of America. pp. 3:1–398.

Chabot N. L. and Drake M. J. 1997. An experimental study of silver and palladium partitioning between solid and liquid metal, with applications to iron meteorites. *Meteoritics & Planetary Science* 32:637–645.

Chabot N. L. and Haack H. 2006. Evolution of asteroidal cores. In *Meteorites and the early solar system II*, edited by Lauretta D. S. and McSween Jr. H. Y. Tucson, AZ: The University of Arizona Press. pp. 747–771.

Chabot N. L. and Jones J. H. 2003. The parameterization of solid metal-liquid metal partitioning of siderophile elements. *Meteoritics & Planetary Science* 38:1425–1436.

Chabot N. L., Campbell A. J., Jones J. H., Humayun M., and Agee C. B. 2003. An experimental test of Henry's Law in solid metal-liquid metal systems with implications for iron meteorites. *Meteoritics & Planetary Science* 38:181–196.

Chabot N. L., Draper D. S., and Agee C. B. 2005. Conditions of core formation in the Earth: Constraints from nickel and cobalt partitioning. *Geochimica et Cosmochimica Acta* 69:2141–2151.

Chabot N. L., Campbell A. J., Jones J. H., Humayun M., and Lauer H. V. 2006. The influence of carbon on trace element partitioning behavior. *Geochimica et Cosmochimica Acta* 70:1322–1335.

Chabot N. L., Saslow S. A., McDonough W. F., and McCoy T. J. 2007. The effect of Ni on element partitioning during iron meteorite crystallization. *Meteoritics & Planetary Science* 42:1735–1750.

Chabot N. L., Saslow S. A., McDonough W. F., and Jones J. H. 2009. An investigation of the behavior of Cu and Cr during iron meteorite crystallization. *Meteoritics & Planetary Science* 44:505–519.

Corrigan C. M., Chabot N. L., McCoy T. J., McDonough W. F., Watson H. C., Saslow S. A., and Ash R. D. 2009. The iron-nickel-phosphorus system: Effects on the distribution of trace elements during the evolution of iron meteorites. *Geochimica et Cosmochimica Acta* 73:2674–2691.

Cottrell E., Walter M. J., and Walker D. 2009. Metal-silicate partitioning of tungsten at high pressure and temperature: Implications for equilibrium core formation in Earth. *Earth and Planetary Science Letters* 281:275–287.

Gessmann C. K. and Rubie E. D. C. 2000. The origin of the depletions of V, Cr, and Mn in the mantles of the Earth and Moon. *Earth and Planetary Science Letters* 184:95–107.

Hillgren V. J., Gessmann C. K., and Li J. 2000. An experimental perspective on the light element in Earth's core. In *Origin of the earth and moon*, edited by Canup R. M. and Righter K. Tucson, AZ: The University of Arizona Press. pp. 245–263.

Humayun M., Keil K., and Bischoff A. 2009. Siderophile elements in metal from Northwest Africa 2526, and enstatite chondrite partial melt residue. 40th Lunar and Planetary Science Conference. p. 1744.

Jochum K. P. and Stoll B. 2008. Reference materials for elemental and isotopic analyses by LA-(MC)-ICP-MS: Successes and outstanding needs. In *Laser-ablation-ICP-MS in the earth sciences: Current practices and outstanding issues*, edited by Sylvester P., Chapter 10, Vancouver, B.C.: Mineralogical Association of Canada Short Course 40. pp. 147–168.

Jones J. H. and Drake M. J. 1983. Experimental investigations of trace element fractionation in iron meteorites, II: The influence of sulfur. *Geochimica et Cosmochimica Acta* 47:1199–1209.

Kegler Ph., Holzheid A., Frost D. J., Rubie D. C., Dohmen R., and Palme H. 2008. New Ni and Co metal-silicate partitioning data and their relevance for an early terrestrial magma ocean. *Earth and Planetary Science Letters* 268: 28–40.

Keil K. 1989. Enstatite meteorites and their parent bodies. *Meteoritics* 24:195–208.

Lehner S. W., Buseck P. R., and McDonough W. F. 2010. Origin of kamacite, schreibersite and perryite in metal-sulfide nodules of the enstatite chondrite Sahara 97072 (EH3). *Meteoritics & Planetary Science* 45:289–303.

Li J. and Agee C. B. 1996. Geochemistry of mantle-core differentiation at high pressure. *Nature* 381:686–689.

Li J. and Agee C. B. 2001. The effect of pressure, temperature, oxygen fugacity and composition on partitioning of nickel and cobalt between liquid Fe-Ni-S alloy and liquid silicate: Implications for the Earth's core formation. *Geochimica et Cosmochimica Acta* 65:1821–1832.

Lin Y. and El Goresy A. 2002. A comparative study of opaque phases in Qingzhen (EH3) and MacAlpine Hills 88136 (EL3): Representatives of EH and EL parent bodies. *Meteoritics & Planetary Science* 37:577–599.

Lin J.-F., Campbell A. J., and Heinz D. L. 2003. Static compression of iron-silicon alloys: Implications for silicon in the Earth's core. *Journal of Geophysical Research—Solid Earth* 108, No. B1, 2045.

Malvin D. J., Jones J. H., and Drake M. J. 1986. Experimental investigations of trace element fractionation in iron meteorites. III: Elemental partitioning in the system Fe-Ni-S-P. *Geochimica et Cosmochimica Acta* 50:1221–1231.

Massalski T. B. 1990. *Binary alloy phase diagrams*. Ohio: ASM International, Materials Park.

McCoy T. J. and Haack H. 2003. Iron and stony-iron meteorites. In *Meteorites, comets, and planets*, edited by Davis A. M. vol. 1 Treatise on Geochemistry, Oxford: Elsevier-Pergamon. pp. 325–345.

McCoy T. J., Dickinson T. L., and Lofgren G. E. 1999. Partial melting of the Indarch (EH4) meteoirte: A textural, chemical, and phase relations view of melting and melt migration. *Meteoritics & Planetary Science* 34:735–746.

Mittlefehldt D. W. 2003. Achondrites. In *Meteorites, comets, and planets*, edited by Davis A. M. vol. 1 Treatise on Geochemistry, Oxford: Elsevier-Pergamon. pp. 291–324.

van Niekerk D., Humayun M., and Keil K. 2009. In situ determination of siderophile trace elements in EL3 meteorites. 40th Lunar and Planetary Science Conference. p. 2049.

Raghavan V. 1988. *Phase diagrams of ternary iron alloys*. The Indian Institute of Metals: Calcutta.

Righter K. and Drake M. J. 1999. Effect of water on metal-silicate partitioning of siderophile elements: A high pressure and temperature terrestrial magma ocean and core formation. *Earth and Planetary Science Letters* 171:383–399.

Righter K. and Drake M. J. 2003. Partition coefficients at high pressure and temperature. In *The mantle and core*, edited by Carlson R. W. vol. 2 Treatise on Geochemsitry, Oxford: Elsevier-Pergamon. pp. 425–449.

Righter K., Drake M. J., and Yaxley G. 1997. Prediction of siderophile element metal/silicate partition coefficients to 20 GPa and 2800°C: The effects of pressure, temperature, oxygen fugacity and silicate and metallic melt compositions. *Physics of the Earth and Planetary Interiors* 100:115–134.

Ulff-Møller F. 1998. Effects of liquid immiscibility on trace element fractionation in magmatic iron meteorites: A case study of group IIIAB. *Meteoritics & Planetary Science* 33:207–220.

Wade J. and Wood B. J. 2005. Core formation and the oxidation state of the Earth. *Earth and Planetary Science Letters* 236:78–95.

Walker R. J., McDonough W. F., Honesto J., Chabot N. L., McCoy T. M., Ash R. D., and Bellucci J. J. 2008. Origin and chemical evolution of Group IVB iron meteorites. *Geochimica et Cosmochimica Acta* 72:2198–2216.

Walter M. J., Newsom H. E., Ertel W., and Holzheid A. 2000. Siderophile elements in the Earth and Moon: Metal/silicate partitioning and implications for core formation. In *Origin of the earth and moon*, edited by Canup R. M. and Righter K. Tucson: The University of Arizona Press. pp. 265–289.

Willis J. and Goldstein J. I. 1982. The effects of C, P, and S on trace element partitioning during solidification in Fe-Ni alloys. Proceedings, 13th Lunar and Planetary Science Conference Part I, *Journal of Geophysical Research* 87(Suppl):A435–A445.